American Mineralogist, Volume 93, pages 1519–1529, 2008

Dissolution-reprecipitation of zircon at low-temperature, high-pressure conditions (Lanzo Massif, Italy)

Daniela Rubatto,[1,*] Othmar Müntener,[2] Auke Barnhoorn,[1,†] and Courtney Gregory[1]

[1]Research School of Earth Sciences, The Australian National University, Canberra 0200 ACT, Australia
[2]Institute of Mineralogy and Geochemistry, University of Lausanne, CH-1015 Lausanne, Switzerland

Abstract

An eclogite facies meta-plagiogranite from the Lanzo massif (western Alps, Italy) contains crystals of zircon intimately associated with allanite. Zircon displays different microtextures ranging from pristine, euhedral, and magmatic to fractured, porous varieties with mosaic zoning, and pervasive recrystallization into euhedral microcrystals. Fractures and voids in the recrystallized zircon microcrystals are mainly filled by high-pressure Na-rich pyroxene. Electron backscattered diffraction analysis revealed a similar crystallographic orientation for primary magmatic zircon crystals and microcrystals, with less than 2° misorientation among neighboring microdomains. The textural change is coupled with chemical and isotopic modifications: recrystallized zircon domains contain significantly less Th and light- to mid-REE, but are richer in Sr than magmatic zircon crystals. Magmatic zircon preserves the protolith U-Pb age of 163.5 ± 1.7 Ma, whereas zircon microcrystals have a mean age of 55 ± 1 Ma. The coexisting allanite also contains inclusions of Na-rich pyroxene and has chemical features (elevated Sr and Ni contents and lack of Eu anomaly) indicating formation at high pressure. Despite being associated texturally with zircon, allanite yields a younger Th-Pb age of 46.5 ± 3.0 Ma, suggesting that the Lanzo unit remained at relatively high pressure conditions for ~8 m.y.

Zircon recrystallization proceeded with volume reduction and loss of material to an alkaline metamorphic fluid that acted as the agent for a coupled dissolution-reprecipitation process. Recrystallization occurred with minimum transport, in a low-strain environment, and was not significantly enhanced by metamictization. The source of the fluid for zircon recrystallization is most probably related to prograde devolatilization reactions in the surrounding serpentinite.

Keywords: U-Th-Pb geochronology, allanite, EBSD, plagiogranite, Lanzo peridotite

Introduction

Zircon is undoubtedly the most important mineral for geochronology and is becoming increasingly important for isotopic tracing (e.g., Hf and O isotopes). Paramount for the correct interpretation of U-Pb ages and isotopic data from zircon is the knowledge of the processes that led to zircon formation and isotopic resetting. Zircon formation via igneous crystallization is dominated by the solubility of Zr in the melt (Watson and Harrison 1983), i.e., when saturation is reached, new zircon will crystallize. During metamorphism, the behavior of zircon is more complex and depends on several factors—not only does zircon precipitate from anatectic melts (e.g., Vavra et al. 1996), but also it possibly grows from the release of Zr from other phases (Bingen et al. 2001; Degeling et al. 2001), or recrystallizes and thus changes its isotopic composition under the influence of fluids and/or deformation (Geisler et al. 2003b; Hoskin and Black 2000; Liermann et al. 2002; Reddy et al. 2006; Rubatto and Hermann 2003; Tomaschek et al. 2003). Therefore, the behavior of zircon during prograde metamorphism, anatexis, and/or hydrothermal alteration has been the subject of intense study (Geisler et al. 2007; Harley et al. 2007; Rubatto and Hermann 2007).

In recent years, studies of low-temperature–high-pressure rocks, mainly eclogites (Liermann et al. 2002; Rubatto et al. 1998, 1999; Rubatto and Hermann 2003; Spandler et al. 2004; Tomaschek et al. 2003), and low-grade metasediments (Rasmussen 2005) have shown that zircon may form and react at relatively low metamorphic temperatures (250–600 °C). At these conditions, zircon recrystallization cannot be attributed to solubility in melts, but requires a subsolidus mechanism (Geisler et al. 2007, 2003b; Tomaschek et al. 2003). Two such mechanisms have been identified: one due to diffusion-reaction and the other due to coupled dissolution-reprecipitation (see a review in Geisler et al. 2007). Recrystallization by diffusion-reaction mainly occurs in metamict, amorphous zircon and is enhanced by fluids. Radiation damage following the radioactive decay of U and Th has long been identified as the main cause for structural and chemical modifications of zircon in the solid-state (Pidgeon et al. 1966). This mechanism has been recently studied in detail experimentally (Geisler et al. 2003a, 2003b). On the other hand, recrystallization of a pristine, non-metamict, but trace-element-rich zircon has been observed in nature and attributed to a dissolution-reprecipitation process that requires fluids or melts (Tomaschek et al. 2003). It has been proposed (Geisler et al. 2007) that the two processes can be distinguished partly on the basis of textures, internal zoning, and composition of the recrystallized zircon. However, particularly for the

* E-mail: daniela.rubatto@anu.edu.au
† Present address: Department of Earth Sciences, Faculty of Geosciences, Utrecht University, 3508 TA Utrecht, The Netherlands.

dissolution-reprecipitation process, detailed studies of natural cases are limited (Tomaschek et al. 2003) and many aspects of this process, such as pressure-temperature conditions, fluid composition, and the role of deformation are poorly understood. Knowledge of these aspects has an important bearing on the interpretation of the age and isotopic information obtained from recrystallized zircon.

We investigate here a case of zircon that preserves unusual recrystallization textures in a rock that experienced relatively low-temperature and high-pressure metamorphism. We show that sub-solidus recrystallization by dissolution-reprecipitation, under the influence of metamorphic fluids, is the principal process by which these unusual zircon textures may be explained. The role of deformation as well as the nature and origin of the fluids is also discussed.

Geological background and sample description

The Lanzo massif is part of the Western Alps blueschist-to-eclogite facies belt and is located in northwestern Italy. The core of the Lanzo massif is dominated by fertile plagioclase lherzolite and minor volumes of spinel harzburgite and dunite (Boudier 1978; Müntener and Piccardo 2003; Piccardo et al. 2004). The borders of the Lanzo massif are marked by strongly foliated serpentinites, which are the combined result of ocean-floor alteration and Alpine high-pressure metamorphism. Locally, the massif is overlain by minor ophicarbonates, MORB-type volcanic rocks, and metasediments (Lagabrielle et al. 1989; Pelletier and Müntener 2006). The massif contains numerous MORB-type mafic dikes and sills (Boudier 1978; Boudier and Nicolas 1972; Kaczmarek et al. 2008) ranging from primitive troctolitic cumulates to highly differentiated Fe-Ti gabbros and plagiogranites (Kaczmarek et al. 2008). U-Pb age determinations of magmatic zircon crystals in different Fe-Ti gabbros provided ages of 158–163 Ma (Kaczmarek et al. 2008). Many gabbroic dikes were metamorphosed during ocean floor alteration and subsequently transformed into eclogites during Alpine subduction (Kienast and Pognante 1988; Pelletier and Müntener 2006). Thermodynamic calculations on talc-chloritoid-kyanite-garnet paragenesis in eclogitized metagabbros gave temperatures of 550–620 °C and pressures of 2.0–2.5 GPa (Pelletier and Müntener 2006).

The sample studied here is a metamorphosed plagiogranite from the southern part of the Lanzo massif (Val della Torre). Plagiogranites form dikes of less than 10 cm thickness, and display sharp contacts with the host serpentinized peridotite. The metamorphosed plagiogranites contain variable proportions of omphacite, (clino-)zoisite, chlorite, jadeite, quartz, allanite, rutile, and locally high concentrations of zircon crystals intergrown with fluorapatite (for details see Kaczmarek et al. 2008). The particular sample studied here (La-VdT-2) is almost entirely composed of jadeite and minor amount of omphacite, allanite-epidote, zircon, fluorapatite, and retrograde analcime, biotite, and albite. There are no precise *P-T* determinations for this particular sample because its limited paragenesis does not permit thermodynamic calculations, but it is reasonable to assume that the *P-T* conditions determined by Pelletier and Müntener (2006) also apply to the metamorphosed plagiogranites.

Sample preparation and characterization

Zircon and allanite grains were prepared as mineral separates, mounted in epoxy and polished down to expose the grain centers. Secondary electron (SE) and cathodoluminescence (CL) investigation was carried out at the Electron Microscope Unit, ANU, with a HITACHI S2250-N scanning electron microscope working at 15 kV, ~60 µA and ~20 mm working distance. High-contrast backscattered electron (BSE) images were obtained with a Cambridge S360 scanning electron microscope using a voltage of 20 kV, current of ~2 nA and a working distance of 15–20 mm.

Crystallographic orientations in the zircon grain were determined at ANU by electron backscatter diffraction (EBSD) on a JEOL6400 SEM working at 25 kV, with a working distance of 23 mm and a 70° sample tilt. The measurements were performed on a zircon section embedded in epoxy and polished to an ultra-fine grade using colloidal silica (particle size 25 nm) and coated with ~4 nm of carbon. Automated beam scan analyses were performed to produce a detailed orientation map of the zircon grain using a step size 0.7 µm. The HKL software Channel 5 was used to collect, index, and analyze the obtained EBSD patterns. For indexing, a zircon structure factor file was generated using the zircon crystallography, space group, and unit cell parameters (Hazen and Finger 1979). This zircon structure file is identical to file 5260 in Reddy et al. (2008), which gave the most reliable pattern indexing in their study. Indexed EBSD patterns resulting in non-reliably indexed measurements (mean angular deviation MAD >1°) were discarded. Such unreliable values include measurements performed on mineral inclusions such as Na-pyroxene and the laser ablation pit. Noise reduction of the data using a wild-spike correction and nearest neighbor correction method removed the majority of unreliable measurements.

The major-element compositions of mineral inclusions in allanite and zircon were determined on a JEOL 6400 SEM (Electron Microscopy Unit, ANU) using an accelerating voltage of 15 kV and a beam current of 1 nA. The composition of Na-pyroxene in the matrix was determined by wavelength dispersive analysis using a five-spectrometer JEOL JXA-8200 electron microprobe at the University of Lausanne. Operating conditions were 15 kV and 10 nA, with a beam size of 1–3 µm. Counting times were 10 s for the alkalis and 15–20 s for other elements. Natural silicates and oxides were used as standards.

Allanite was analyzed with a Cameca SX100 electron microprobe at the Research School of Earth Sciences (RSES), ANU, working at 15 kV and 20 nA, with a defocused electron beam of 5 µm. Details of EMP analytical protocols for allanite are reported in Gregory et al. (2007).

Trace-element analyses of zircon and allanite mineral separates used for age determinations were performed by laser ablation–ICP-MS at the RSES using a pulsed 193 nm ArF Excimer laser with 100 mJ energy at a repetition rate of 5 Hz (Eggins et al. 1998) coupled to an Agilent 7500 quadrupole ICP-MS with a spot size of 23 and 32 µm. External calibration was performed relative to NIST 612 glass. Internal standards were Ce for allanite, as measured by EMP, and stoichiometric Si for zircon. During the time-resolved analysis of minerals, contamination resulting from inclusions, fractures, and zones of different composition was monitored by several elements and only the relevant part of the signal was integrated. For the mosaic-zoned zircon domains, in particular contamination by inclusions was common and generally easily detectable by high Ca (Na-pyroxene and allanite) or P (fluorapatite) contents.

Analyses of U-Th-Pb isotopes were performed using the SHRIMP RG sensitive, high-resolution ion microprobe at the RSES using a 3.5–4.0 nA, 10 kV primary O_2^- beam focused through a 120 µm aperture to form a ~25 µm diameter spot. Data acquisition for zircon followed Williams (1998): the measured $^{206}Pb/^{238}U$ ratio was corrected using reference zircon TEMORA (Black et al. 2003), and the U concentration was corrected using the SL 13 zircon. Single ages are quoted as $^{206}Pb/^{238}U$ ages corrected for common Pb using the measured $^{207}Pb/^{206}Pb$ according to Williams (1998) and the model common Pb composition of Stacey and Kramers (1975). Average ages are intercept ages in the uncorrected $^{207}Pb/^{206}Pb$ vs. $^{238}U/^{206}Pb$ diagram. Intercepts were forced to the model common Pb because of the limited dispersion of the data along the chord. Such intercept ages are identical within error to the average of the corrected $^{206}Pb/^{238}U$ ages.

The analytical procedure for allanite was described by Gregory et al. (2007). The Lanzo allanite was mounted with CAP as the Th-Pb standard, with an assumed $^{208}Pb/^{232}Th$ ratio of 0.0137 ± 0.0002 (275.6 Ma; Barth et al. 1994), as well as two secondary standards (AVC and Tara). The samples were run in a round-robin, with CAP analyzed every fourth analysis. The CAP standard calibration was reproducible to 2%. AVC and Tara produced Th-Pb SHRIMP ages of 279.8 ± 2.7 Ma (MSWD 0.9) and 414.6 ± 4.3 Ma (MSWD 0.4), which were identical to their respective ID-TIMS ages (Gregory et al. 2007). No significant matrix effect was observed

for the calibration of the Lanzo allanite using the CAP standard.

Age calculation was done using the software Isoplot/Ex (Ludwig 2003) for zircon and RSES internal software for allanite. Isotopic ratios and single ages are reported with 1σ errors, whereas mean ages are given at the 95% confidence level.

Zircon description

The sample La-VdT-2 contains large (several hundred micrometers across) zircon crystals, which are rarely euhedral, but in most cases display some crystals faces along with sharp edges. In hand sample, most crystals are opaque, milky to gray in color, and have an extremely rugged surface with visible voids and semi-inclusions of other minerals. In thin section, most zircon crystals are rich in dark microinclusions and pores. Zircon crystals are texturally associated with the high-pressure paragenesis including Na-rich pyroxene and allanite (Fig. 1), with which they may have irregular (serrated) boundaries.

Internal texture and zoning

The internal texture of the zircon was investigated in detail by SEM imaging of the mineral separate. A transition among euhedral, inclusion-free zircon, and inclusion-rich zircon was observed. The transition can be described in a series of steps. A network of fractures filled by metamorphic minerals (i.e., Na-rich pyroxene and epidote) develops within the pristine, inclusion-free, magmatic crystal (Figs. 2a–2c). The network of filled fractures may comprise a significant volume of the crystal (20% in two dimensions, Fig. 2b). The increase in density of fractures leads to the formation of irregular "islands" of zircon, in some cases with dendritic shapes surrounded by metamorphic minerals. These islands have variable size (a few to several tens of micrometers), become increasingly euhedral, and transform into porous aggregates of zircon microcrystals with an average size of 10 µm (Figs. 2e–2f). These aggregates range from grain- to inclusion-supported, where the interstices are filled with metamorphic minerals (see below for details). Individual zircon microcrystals are, however, free of inclusions and pores. Porosity (presence of voids that can be filled by metamorphic minerals) is clearly associated with the transition toward aggregates of zircon microcrystals. Within a single grain, inclusion-free pristine zircon and aggregates of zircon microcrystals both can be present.

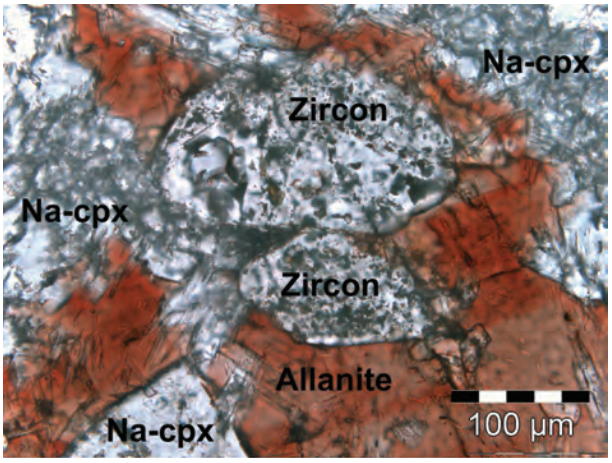

Figure 1. Photomicrograph of sample La-VdT-2 showing textural relationships among zircon, allanite, and high-pressure Na-pyroxene (Na-cpx).

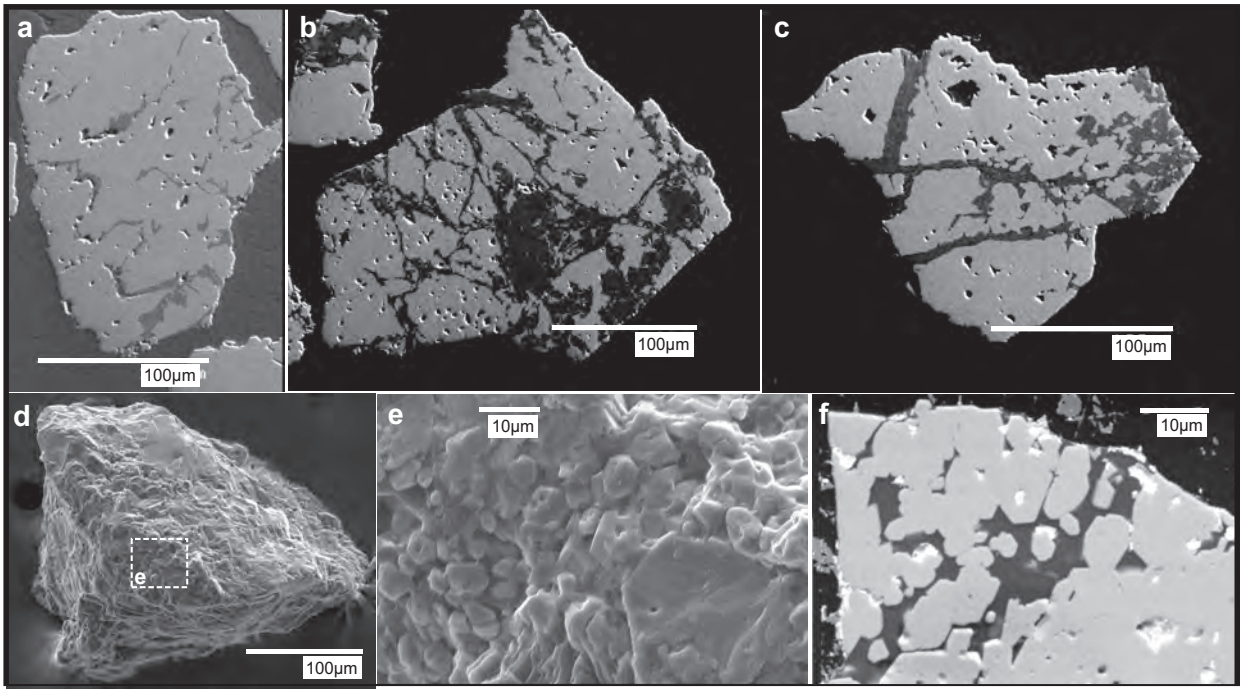

Figure 2. Secondary electron images of zircon crystals. (**a**–**c**) Progressive fracturing of the original magmatic crystals leading to isolated zircon islands and microcrystals (**b** and **c**) in the proximity of the fractures. The mineral that fills the fractures is mainly Na-rich pyroxene. (**d**–**f**) Formation of euhedral zircon microcrystals. Note that **e** is a detail of **d**. White speckles in **f** are relict of gold coating after SHRIMP analysis. **a**–**c** and **f** are images of a polished zircon surface embedded in epoxy resin, whereas **d** and **e** are images of a free-standing crystal.

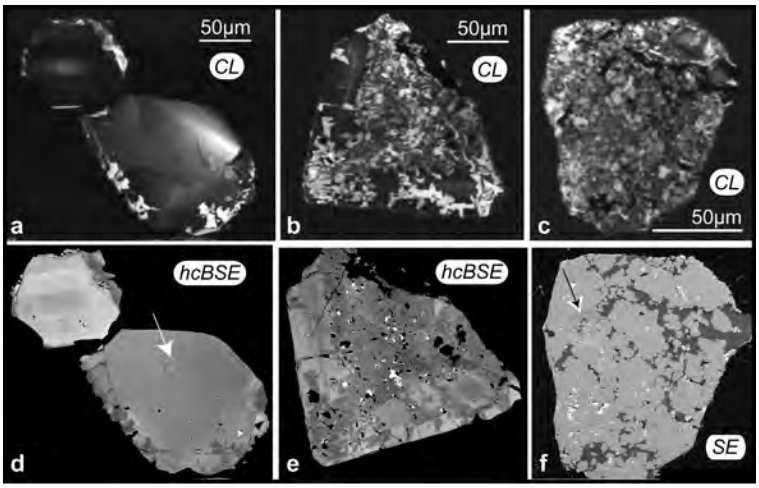

FIGURE 3. Progressive changes in zircon internal structure denoted by changes in CL zoning from broad oscillatory to mosaic and in BSE emission, together with increased fracturing, porosity, and inclusions. (**a** and **d**) Nearly pristine magmatic crystal with signs of recrystallization along the rim and fractures. (**b** and **e**) Crystal preserving euhedral faces and magmatic zoning in the external part, but with intense recrystallization in the central part. (**c** and **f**) Completely recrystallized crystal comprising an aggregate of zircon microcrystals. Inclusions are mainly Na-rich pyroxene and epidote. Bright speckle in **e** and **f** are relicts of gold coating after SHRIMP analysis. SHRIMP pits are visible in **d** and **f** as indicated by the arrow. Type of image: CL = cathodoluminescence, hcBSE = high-contrast, back-scattered electrons, SE = secondary electrons.

With the fracturing and formation of zircon microcrystals, the external surface of the crystals becomes increasingly irregular and etched (Fig. 2d). Even when the process of formation of zircon microcrystals is dominant, the overall size of the crystal is maintained, together with some straight faces and sharp edges (Figs. 2b, 2c, and 2f).

The textural transformation of the zircon is associated with a change in cathodoluminescence (CL) zoning. The magmatic crystals preserve the internal sector or broad-band planar zoning, which is progressively transformed into fine, mosaic-like, irregular zoning (Figs. 3a–3c). The transformation initiates along fractures and at grain boundaries, and progressively "consumes" the crystals leaving isolated domains where the planar zoning is still visible (Fig. 3b). In the hundreds of crystals investigated for this study, the mosaic is the dominant zoning type. In ca. 50% of the crystals, no significant relict of the magmatic zoning is preserved. Aggregates of zircon microcrystals always have an intense mosaic zoning in CL. By comparing secondary electron and CL images, it appears that the transformation into mosaic zoning precedes the formation of zircon microcrystals. Domains with mosaic zoning might not develop zircon microcrystals, but display only fracturing and chemical changes (compare Figs. 3b and 3e). The correlation between CL zoning and zircon transformation is to be expected because CL emission mainly reflects compositional variations (Hanchar and Miller 1993), whereas structural variations such as defects and deformations are second-order effects (e.g., Reddy et al. 2006).

Back-scattered electron (BSE) emission is quantitatively correlated to average atomic number (Z), and therefore depends exclusively on the composition of the material. In high-contrast BSE (hcBSE, Figs. 3d–3e), the difference between the magmatic zircon domains and the domains with mosaic zoning is obvious and marked by a decrease in emission, i.e., decrease in average Z. From the detailed comparison of CL and hcBSE images, it appears that both techniques show the same features in an inverse fashion: high CL emission corresponds to low BSE emission. The contrast in CL emission is stronger and easier to detect with a common SEM and therefore CL images are here used to depict the zircon chemical zoning.

Internal structure: EBSD

EBSD mapping was performed on one zircon crystal displaying mosaic zoning and advance transformation to microcrystals (Fig. 4). The EBSD investigation focused on a portion of the zircon where a transition from a large zircon crystal (upper part of the crystal in Fig. 4) to an aggregate of zircon microcrystals (lower part of the crystal) is observable.

Most of the zircon grain has the same crystallographic orientation (pink color in Fig. 4b), which is defined as the "original" orientation, taken to represent the orientation of the large zircon crystal. In the bottom half of the grain, where zircon microcrystals are present, the majority of the area has orientations that deviate slightly from the original orientation. There is a gradual change in orientation from the top to the bottom of the measured area (rendered as change in pink color in Fig. 4b). The maximum misorientation angle is ~20° (Fig. 4c), achieved by gradual small angle misorientations from the top to the bottom of the zircon. Neighboring domains have misorientations of <2°. A few areas in the bottom half of the sample have orientations that are unrelated to the original orientation of the zircon grain (Fig. 4c) resulting in large misorientation angles with respect to the other areas in the zircon. The areas with unrelated crystallographic orientations correspond to euhedral micrograins adjacent to omphacite inclusions.

The lack of significant misorientations between different areas of a mosaic-zoned crystal has been confirmed in another zircon grain for which spot EBSD analyses were measured but no detailed map was acquired.

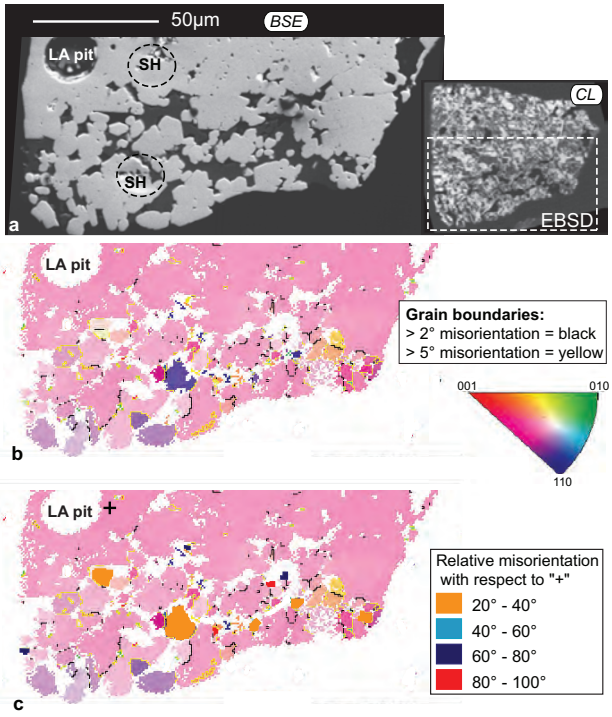

FIGURE 4. (**a**) Low-contrast BSE image of zircon analyzed by EBSD. The LA-ICPMS (LA pit) and SHRIMP U-Pb pits (SH) are visible. The SHRIMP analysis partly sitting on a Na-rich pyroxene inclusion (lower part) contained a high proportion of common Pb (40%) and was thus discarded. The inset shows the CL image of the entire crystal before analysis. (**b**) EBDS map showing the crystal orientation and with superimposed the boundaries between grains that differ in orientation of more than 2° and 5°. (**c**) EBSD map showing the misorientation of the different domains with respect to a reference point (+). See text for discussion.

COMPOSITION OF ZIRCON AND ITS INCLUSIONS

The different zircon domains have been investigated for their trace-elements and isotopic compositions (U-Pb) to determine the effect of the recrystallization process on chemistry, and the temperature and time at which recrystallization occurred. To provide constraints on the *P-T* conditions of formation, the inclusions found in zircon have been compared with those of the matrix minerals.

Zircon trace-element composition

There is a significant difference in trace element composition between zircon with planar zoning and zircon domains with mosaic zoning the latter including both zircon microcrystals as well as fractured and recrystallized domains (Fig. 5; Appendix 1[1]). The planar-zoned crystals are richer in Th at similar U contents, resulting in a higher Th/U ratio (mostly around 2.0) compared to the Th/U <1 (0.05–0.9) in the mosaic zircon (Fig. 5a). With respect to magmatic zircon, mosaic domains are richer in Sr (2.4–4.0 vs. 0.6–1.8 ppm) and generally poorer in L-MREE. In the chondrite-normalized REE patterns, the mosaic domains show a stronger depletion in MREE with respect to the HREE (Figs. 5b–5c). Both domains have a weak negative Eu-anomaly, which is more pronounced in the mosaic domains (Eu/Eu* 0.4–0.6) than in the planar domains (Eu/Eu* 0.6–0.9).

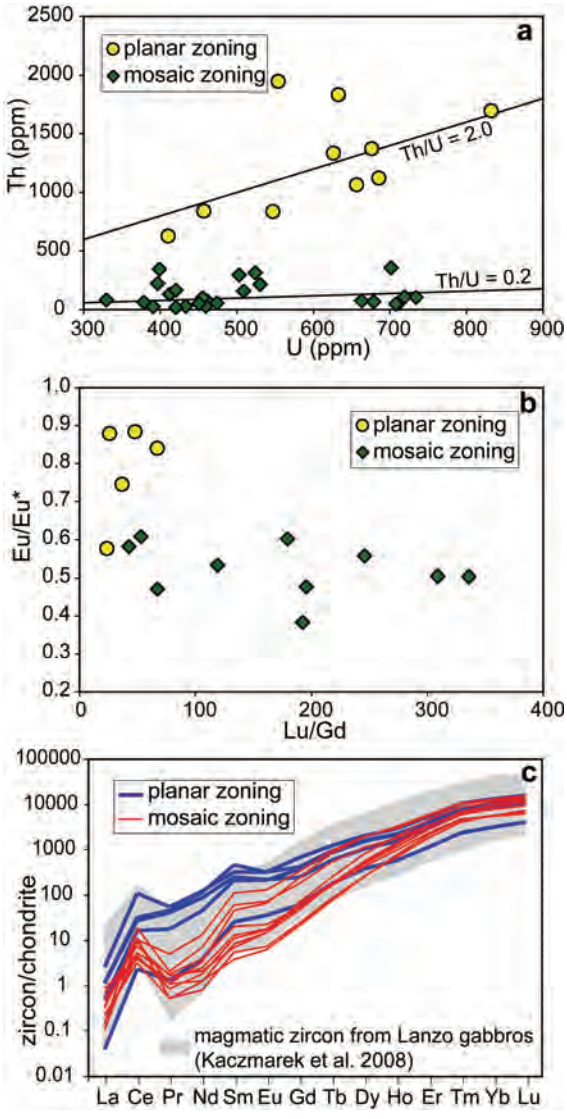

FIGURE 5. Zircon chemical composition. (**a**) Thorium vs. U content for magmatic and metamorphic (mosaic zoning) zircon domains. Data are from LA-ICPMS and SHRIMP analyses. A few analyses with higher Th and U plots outside the area shown. (**b**) Europium anomaly vs. Lu/Gd as an indicator of the steepness of the REE pattern. Ratios are from chondrite-normalized values. (**c**) Chondrite normalized REE patterns of planar- and mosaic-zoned zircons from the investigated sample compared to magmatic zircon from the Lanzo gabbros. See text for discussion.

Zircon U-Pb age

The isotopic composition of the zircon (Appendix 2[1]) follows the domains observed in CL. The crystals or crystal domains that

[1] Deposit item AM-08-049, Appendices 1–6. Deposit items are available two ways: For a paper copy contact the Business Office of the Mineralogical Society of America (see inside front cover of recent issue) for price information. For an electronic copy visit the MSA web site at http://www.minsocam.org, go to the American Mineralogist Contents, find the table of contents for the specific volume/issue wanted, and then click on the deposit link there.

best preserve the planar zoning yielded the older ages with a cluster of 9 analyses at 163.5 ± 1.7 Ma (mean squared weighted deviates, MSWD = 1.8, Fig. 6). Domains with mainly mosaic zoning scatter in apparent age between 132 and 52 Ma. Of these, the oldest ages (132–67 Ma) correspond to crystals with relics of planar zoning without aggregates of zircon microcrystals. These ages are thus expected to represent a mixing between magmatic and recrystallized zircon (see also Tomaschek et al. 2003). The remaining 16 analyses correspond to domains where there is advanced transformation into microcrystals and thus recrystallization was pervasive. They define an age of 54.7 ± 0.8 Ma with a relatively large spread (MSWD = 3.9). The exclusion of the three most extreme data points reduces the spread (MSWD = 1.9 on 13 analyses) without changing significantly the age (54.9 ± 0.7 Ma, Fig. 6). Therefore, an age of 55 ± 1 Ma is taken as the best age estimate for the crystallization of the zircon microcrystals. The spread observed in the data can either be attributed to a combination of Pb loss and small-scale inheritance, or it could be the reflection of a prolonged recrystallization process.

Due to the small size of the zircon microcrystals, SHRIMP analyses occasionally overlapped with the interstitial inclusions (mainly Na-rich pyroxene). This overlap was, however, detected by the high proportion of common Pb in such analyses (Na-rich pyroxene is a mineral rich in common Pb). Those analyses have thus been discarded and are not reported in tables and figures.

Inclusion composition

The mosaic-zoned zircon domains are porous and contain abundant voids and mineral inclusions. Whereas the single zircon microcrystals are inclusion-free, the aggregates have interstitial minerals that can also be classified as inclusions (these comprise semi-inclusions, i.e., inclusions not fully enclosed that communicate with the matrix). The inclusions can either be single minerals or aggregates of minerals with dendritic textures (Figs. 7a–7c). Dendritic mineral aggregates are most commonly found in highly fractured mosaic-zoned zircon, but are generally absent within the aggregates of zircon microcrystals.

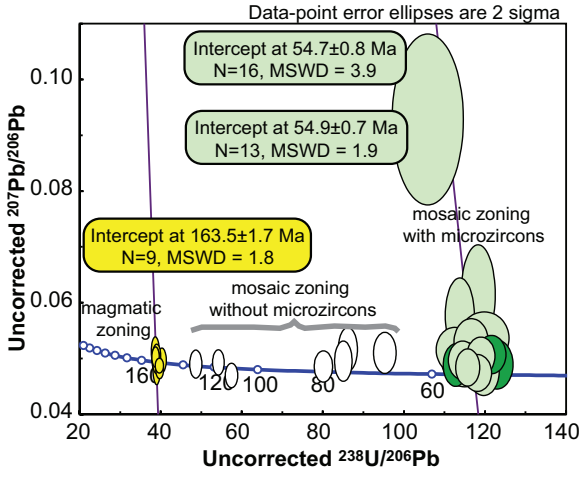

Figure 6. Tera-Wasserburg plot for uncorrected SHRIMP zircon U-Pb analysis. Ages are intercept ages forced to the model common Pb composition of Stacey and Kramers (1975). For the mosaic zircon crystals, two different intercepts are calculated: (1) including all the data points (54.7 ± 0.8 Ma), and (2) excluding three data points (dark green ellipses) that are out of error with intercept 1 and add additional scatter (54.9 ± 0.7 Ma). This exclusion is based on statistics only, as no geological or mineralogical criteria could be adopted. Notably, the two intercepts are the same, within error, and thus an age of 55 ± 1 Ma is adopted (see text for further discussion).

The most common mineral found in these different inclusion settings is Na-pyroxene, with subordinate epidote (rarely allanitic), analcime, and fluorapatite. Na-pyroxene is also found as a common inclusion in the large allanite crystals. The composition of Na-rich pyroxene inclusions in zircon varies over a range of Al/Na, and overlaps with the composition of the Na-rich pyroxene found in the matrix and as inclusions in allanite (Fig. 7d; Appendix 3[1]).

Allanite composition and geochronology

Zircon is intimately associated with allanite, another U-Th mineral. Allanite occurs in a variety of textures: as an interstitial phase among Na-rich pyroxene, associated with zircon (Fig. 1), intergrown with fluorapatite, or as rare inclusions in zircon.

In BSE images, the allanite grains show a broad planar zoning (Fig. 8a) and often display intergrowth textures with Ca-phosphate. Allanite has a constant CaO content of 11.0–12.5 wt%, an Al_2O_3 content between 17.5 and 19.0 wt%, and is poor in FeO (<0.75 apfu, Appendix 4[1]). When compared with magmatic allanite (Gregory et al. 2007), allanite in the Lanzo sample has a moderate Th content (400–1000 ppm, Appendix 5[1]), and is poor in U (~20 ppm) but notably rich in Sr (1.5–3.3 wt%). It is consistently rich in REE (ΣREE ~21–22 wt%) and has a REE pattern with limited depletion of HREE with respect to the LREE $(La/Lu)_N$ = 100–140, and a negligible Eu negative anomaly (Fig. 8b).

Allanite was dated by SHRIMP using the Th-Pb system because of the high content of Th with respect to U. Allanite domains analyzed by SHRIMP (Appendix 6[1]) contain 200–900 ppm Th and a high proportion of common Pb ($^{208}Pb_c$ = 62–88% of the total ^{208}Pb measured), thus making the age calculation strongly dependent on the common Pb composition chosen. Single SHRIMP analyses were corrected using an initial $^{207}Pb/^{206}Pb$ value of 0.864 ± 0.021 (2σ) obtained from the free intercept in a Tera Wasserburg plot of uncorrected Pb/U data (Fig. 8c), and the corresponding $^{208}Pb/^{206}Pb$ value of 2.098. These values are supported by an initial $^{208}Pb/^{206}Pb$ composition of 2.06 ± 0.93, determined from a Th-Pb isochron of uncorrected SHRIMP data. This Pb isotopic composition is similar to the model common Pb composition (Stacey and Kramers 1975); in fact, adopting a 50 Ma model common Pb composition would not change the age. The average $^{232}Th/^{208}Pb$ age of 15 analyses is 46.5 ± 3.0 Ma (95% c.l., MSWD 0.11). One additional analysis was discarded due to an unreasonably large error (>20%).

LA-ICPMS analyses of the same allanite sample returned a spread in Th/Pb ratios allowing an isochron to be defined in $^{232}Th/^{206}Pb$ vs. $^{208}Pb/^{206}Pb$ (see Gregory et al. 2007 for details). The isochron defines an age within error of the SHRIMP age, but much less precise (around 47). The initial $^{208}Pb/^{206}Pb$ value obtained from this isochron is again within error of the composition chosen for correcting the SHRIMP analyses and thus support the chosen common Pb composition.

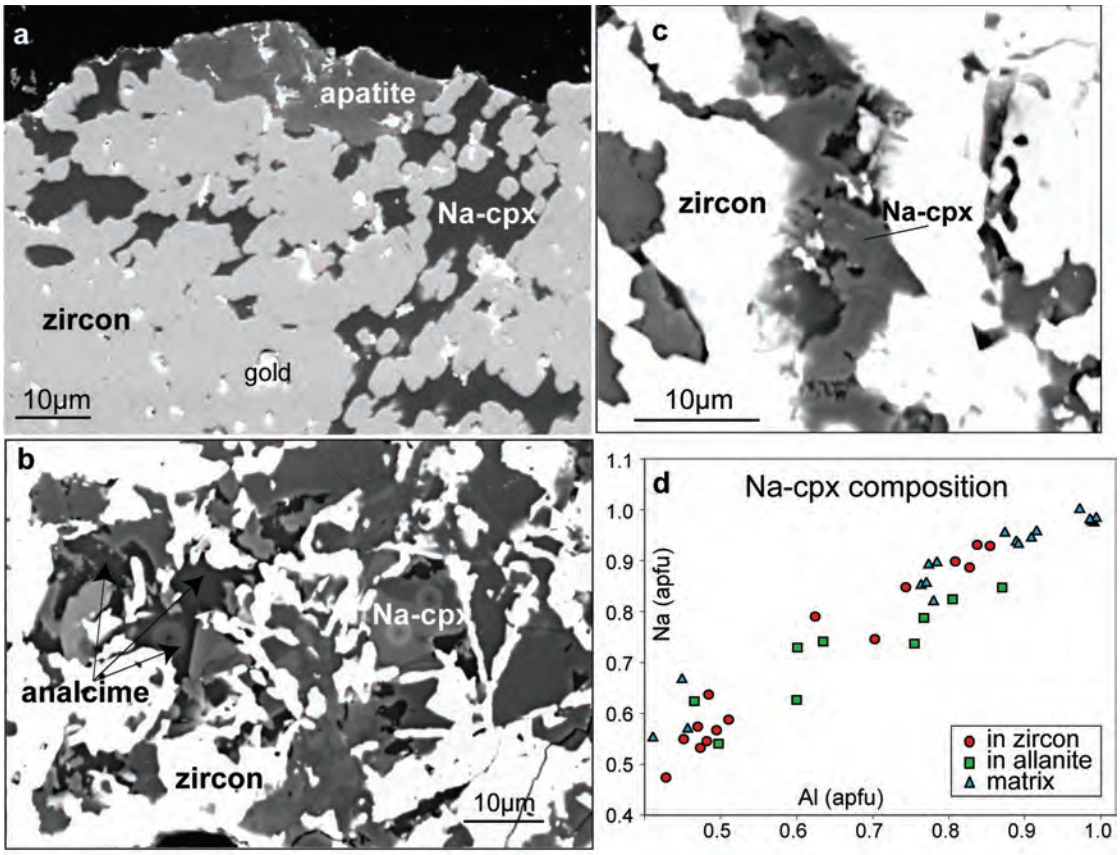

FIGURE 7. Inclusions in zircon. (**a**) BSE image of zircon with advanced formation of microcrystals and abundant inclusions to semi-inclusions of Na-rich pyroxene and fluorapatite. White speckles are relicts of gold coating after SHRIMP analysis. (**b**) BSE image of dendritic zircon with interstitial composite inclusions of zoned Na-rich pyroxene and late analcime. The circular marks correspond to EDS analyses. The different shades of gray in the Na-rich pyroxene correspond to variable CaO content. (**c**) Secondary electron image of polyphase metamorphic mineral inclusions in zircon. The irregular shape of the different phases suggests quenching from a fluid. (**d**) Composition of Na-rich pyroxene found as an inclusion in zircon and allanite and as matrix mineral.

DISCUSSION

Zircon interpretation

The documentation presented above points to two main zircon types in the Lanzo sample: planar-zoned zircon and mosaic-zoned zircon, the latter including the aggregates of zircon microcrystals. The semi-euhedral shape, regular zoning, and high Th/U ratio of the planar-zoned zircon are common to many magmatic zircon crystals, particularly from mafic rocks (e.g., Corfu et al. 2003; Rubatto and Gebauer 2000). In our sample, all zircon domains with these features yielded a Jurassic age averaging at 163.5 ± 1.7 Ma, a common age for mafic intrusives in the Lanzo massif and other Alpine ophiolites (Kaczmarek et al. 2008). These features indicate that this zircon type represents the original magmatic zircon that crystallized in the protolith.

The mosaic-zoned domains are characterized by fracturing and transformation into aggregates of zircon microcrystals, intimately associated with metamorphic minerals such as Na-rich pyroxene, analcime, and epidote. The decrease in trace-element content observed in this zircon type (Fig. 5c) is a characteristic of metamorphic zircon formed at relatively low temperatures (Hoskin and Black 2000; Rubatto 2002). The maximum temperature reached by the Lanzo sample during metamorphism was 550–620 °C (Pelletier and Müntener 2006), below the solidus for this system. The mosaic-zoned domains are significantly younger than the magmatic zircon, and their age falls within the period for Alpine orogeny (see below). Therefore, the metamorphic inclusions, the composition, and the age are evidence that the mosaic zircon formed during Alpine metamorphism.

The recrystallization process

The microtextures observed in the Lanzo zircon crystals are unusual and, at least in its most extreme form (i.e., the aggregates of zircon microcrystals), never documented before (cf. Corfu et al. 2003). Zircon aggregates were previously described by Charoy and Raimbault (1994) in HFSE- and REE-rich differentiates of the Suzhou pluton, China. In that case, however, aggregates of euhedral zircon microcrystals (10–40 µm across) grew on the surface of euhedral, pre-existing large zircon crystals that showed only very limited signs of corrosion. In that case, no specific process was identified for the zircon aggregates other than a "general metasomatism" of the rock. Whereas the aggregates of zircon microcrystals are a new feature, the mosaic zoning described here has been observed previously in crustal rocks (e.g., Corfu et al. 2003; Rubatto et al. 1998; Tomaschek et al. 2003). It is therefore important to understand the recrystalliza-

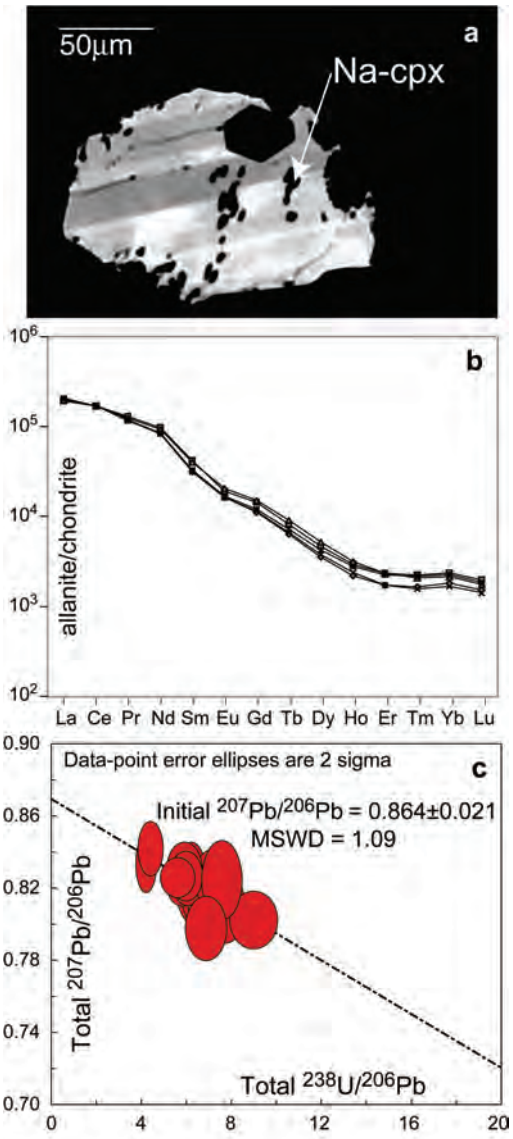

FIGURE 8. (**a**) BSE image of a representative allanite crystal with inclusions of Na-rich pyroxene. (**b**) Chondrite-normalized, trace-element patterns of dated allanite crystals. (**c**) SHRIMP U-Pb analyses of allanite: the intersection of the regression line with the Y-axis defines the composition of common $^{207}Pb/^{206}Pb$ in allanite (see text for age calculation).

tion process that led to this unusual texture to possibly explain this and other cases.

As described above, there is a progressive transformation from planar-zoned, magmatic zircon to mosaic-zoned and inclusion-rich zircon to finally aggregates of zircon microcrystals. The abundant fracturing, mineral inclusions, and voids present in the metamorphic zircon indicate that this transformation is associated with a volume reduction. This can be accommodated by dissolution of zircon into a fluid/melt phase and transport outside the system. The presence of porosity on recrystallization fronts and the loss of material to the fluid is a well-known phenomenon in mineralogy (for a review see Putnis 2002). Porosity has been documented in natural zircon (Geisler et al. 2007; Tomaschek et al. 2003) and has been reproduced in zircon recrystallization experiments (Geisler et al. 2003a). Porosity during recrystallization is commonly associated with abundant mineral inclusions (Geisler et al. 2007; Spandler et al. 2004), as observed in the Lanzo zircon.

The mosaic-zoned domains are also characterized by a decrease in average *Z* (Fig. 3), documented by the decrease in trace elements such as Th and L-MREE (Appendix 1 and Fig. 5c). This is another common feature in zircon that underwent subsolidus recrystallization (Geisler et al. 2003a, 2007; Hoskin and Black 2000; Spandler et al. 2004; Tomaschek et al. 2003). In the case of the Lanzo zircon, the presence of allanite, or some other precursor LREE-rich mineral, could easily account for the depletion of Th and L-MREE in the metamorphic zircon. As explained by Geisler et al. (2007), the occurrence of pores and inclusions at the recrystallization front and the decrease in trace elements are due to the fact that a zircon solid solution (i.e., zircon rich in trace elements) has a higher solubility in the fluid than pure zircon. It follows that zircon formed by dissolution will be poorer in trace elements than the original zircon. According to Geisler et al. (2007), this difference in solubility is the driving force of recrystallization by dissolution-reprecipitation. Geisler et al. (2007) also pointed out that this process can occur regardless of the low solubility of zircon in the fluid. The process described by Geisler et al. (2007) for zircon follows from the work on coupled dissolution-reprecipitation of Harlov et al. (2005) on fluorapatite and monazite as well as that of Putnis and co-workers (Putnis 2002; Putnis and Putnis 2007; Putnis et al. 2005) on other phases.

In the case of the Lanzo zircon, the dissolution-reprecipitation process occurred over short distances (<100 µm) and involved little transport: the zircon microcrystals formed, i.e., precipitated, within the original site of the magmatic zircon. This process is significantly different from one in which transport occurs between dissolution and reprecipitation. This second scenario will produce distinct overgrowths on zircon cores as often seen in high-grade rocks where melt is present (e.g., Corfu et al. 2003; Vavra et al. 1996).

In most natural and experimental studies, recrystallization driven by dissolution-reprecipitation has been observed in highly metamict zircon, whose structure was damaged by radiation decay (Geisler et al. 2003a, 2003b; Pidgeon 1992; Pidgeon et al. 1998). However, a case of fluid-induced recrystallization of non-metamict zircon from the Syros eclogites has been reported by Tomaschek et al. (2003). The magmatic zircon from Lanzo contains moderate to high amounts of radioactive Th and U (this work and Kaczmarek et al. 2008), but were only 105–110 m.y. old when recrystallization occurred. Following the calculation of radiation dose of Ewing et al. (2000), the radiation dose accumulated by the Lanzo zircon over this period is low. A 108 Ma zircon with 400–1000 ppm U and 600–2000 ppm Th will accumulate a dose of 0.014–0.038 displacements per atom (dpa). Different zircon crystals will have significantly different critical amorphization doses due to their thermal evolution, i.e., the dose above which amorphous domains become interconnected creating channels for hydrothermal alteration and infiltration of impurities thus accelerating dissolution (Ewing et al. 2000).

The dose accumulated even in the most radiogenic Lanzo zircon is, however, significantly lower than the critical amorphization dose predicted by most workers (e.g., 0.3–0.5 dpa, see review in Ewing et al. 2000). The radiation dose in the Lanzo zircon appears too low to have produced enough amorphization to favor fluid infiltration and thus was not a likely cause for recrystallization. This conclusion is supported by the fact that preserved magmatic zircon domains do not show evidence of radiation damage (porosity or fracturing) and do not contain high levels of impurities (e.g., <100 ppm of Ca).

In summary, the textural and chemical features of the Lanzo metamorphic zircon indicate that it formed by a dissolution-reprecipitation process acting locally, in the presence of a fluid phase. This process is similar to those described by Tomaschek et al. (2003) and Geisler et al. (2007), with the exception of the end product. For the first time, we can observe the formation of individual, distinct, euhedral new zircon crystals, which are free of porosity and inclusions. These characteristics suggest that the microcrystals are a stable form of metamorphic zircon that has not yet been reached (or yet observed) in the reported cases of mosaic-zoned, porous, or skeletal zircon crystals. We thus propose that in the Lanzo metamorphic zircon, the recrystallization process was more pervasive and reached completion, or at least a stable configuration, in the form of aggregates of zircon microcrystals.

The role of deformation

EBSD can further constrain the recrystallization process. Although the zircon grain has undergone several chemical/physical changes, the majority of the grains, including the microcrystals, have virtually the same orientation. This common orientation is considered the original crystallographic orientation of the magmatic zircon grain. Preservation of crystallographic information between parent and daughter crystals is indeed a recurrent feature in dissolution-reprecipitation reactions (e.g., Putnis and Putnis 2007).

Within the upper part of the investigated area (Fig. 4) there is no formation of subgrains regardless of the fact that the zircon has mosaic zoning. This feature indicates that the mosaic zoning was probably not induced by deformation. Changes in chemistry and CL-zoning, induced by deformation, were instead proposed by Reddy et al. (2006) for a large zircon crystal within a high-temperature shear zone, and, subsequently, has been observed in some zircon crystals from the Lanzo metagabbro (Kaczmarek et al. 2008). The difference here might well be the low temperature of metamorphism in our sample (<600 °C) compared to the temperature of high-grade shearing in the metagabbros (≥800 °C, Kaczmarek et al. 2008).

Two different effects are revealed by EBSD mapping. These include an observed progressive rotation of the crystallographic orientation toward the bottom half of the zircon (Fig. 4b). This rotation is most likely caused by a period of stress-driven deformation where deformation is accommodated by the formation of dislocations within the zircon crystal and between the microcrystals. In the second effect, the euhedral zircon microcrystals show different degrees of misorientation relative to the main crystal (Fig. 4c), mostly below 20°. This feature suggests that there was some degree of randomness during the formation of the microcrystals, but that the new microcrystals mainly inherited the crystallographic orientation of the original zircon. This inheritance is another indication that dissolution and reprecipitation occurred without significant gaps in time and space. Otherwise reorientation of the crystals would be expected. Overall, the weak misorientation relative to the magmatic zircon, and some randomness in the microcrystal orientation suggest that significant strain was lacking during the dissolution-reprecipitation process.

The nature and source of the fluid

There is common agreement that recrystallization processes are strongly enhanced by fluids (Geisler et al. 2003a, 2007; Putnis 2002; Tomaschek et al. 2003). As discussed above, fluids were the main driver of the recrystallization process in the Lanzo zircon, acting as a dissolution and reprecipitation agent. The present rock assemblage consists mainly of anhydrous Na-rich pyroxene. The precursor rock was most likely a plagiogranite, mostly composed of primary anhydrous minerals. As there is no indication of prograde dehydration reactions in this sample, the fluid responsible for the recrystallization process was likely sourced outside the plagiogranite itself. In the Lanzo massif, metagabbros, and plagiogranites occur as dikes within peridotite, which was locally serpentinized. During prograde metamorphism, the Lanzo massif reached conditions at which antigorite + brucite reacted to form olivine + H_2O and thus liberated abundant fluids (Pelletier and Müntener 2006). Migration of such fluids into the plagiogranite dike is a possible cause for zircon recrystallization. The high Ni content of allanite could also be an indication of a peridotitic source for these fluids.

Regardless of the possible origin and initial composition of the fluid, when it reached the plagiogranite, the fluid entered in contact with an extremely Na-rich and thus alkaline environment. Fluids in equilibrium with mafic eclogites have indeed been calculated to be rich in Na, Si, and Al (Manning 2004). The Lanzo zircon crystals were thus in contact with a relatively cold (<600 °C), alkaline, high-pressure fluid. Unfortunately, little is known about the effects of fluid composition, pressure, and temperature on zircon solubility. In their experimental work, Ayers and Watson (1991) concluded that *P* and *T* might have little effect on zircon solubility. Conversely, Liermann et al. (2002) estimated zircon solubility by relating it to the solubility of quartz, and concluded that solubility will increase with *T* and *P*. Zircon solubility in alkaline magmas is higher than in non-alkaline equivalents (Watson and Harrison 1983) and, by analogy, the presence of high amounts of Na would be expected to increase the solubility of Zr in subduction zone fluids. This conclusion is supported by recent experimental work (Ayers, pers. comm.).

High-pressure, alkaline fluids are commonly rich in solutes (Manning 2004). Yttrium, U, and REE-rich inclusions have been identified as another typical sign of recrystallization (e.g., Geisler et al. 2007; Tomaschek et al. 2003), where elements that were leached from the recrystallizing zircon precipitated as inclusions. The absence in the Lanzo zircon of such inclusions might be another indication that the fluid was capable of dissolving and transporting higher amounts of trace elements.

In summary, in the Lanzo sample there is evidence for the presence of solute-rich alkaline fluids at high pressure, which

were capable of dissolving relatively high amounts of trace elements. Such a fluid would have necessarily accelerated the dissolution-reprecipitation process, leading to the formation of stable aggregates of zircon microcrystals.

Zircon and allanite formation at high pressure

Mosaic textured, zircon microcrystals yield an age of 55 ± 1 Ma, whereas allanite yields a significantly younger age of 46.5 ± 3.0 Ma. The U-Pb system in the two minerals thus records separate stages in the metamorphic evolution of the host rock. For zircon, it is reasonable to assume that the determined age dates the formation of the mineral, as Pb diffusion in zircon at these low temperatures is unlikely. For allanite it could be possible that the age is recording a snapshot in the cooling history of the rock. No experimental data are available for Pb diffusion in allanite. A detailed study of zircon and allanite in the Bergell pluton (Oberli et al. 2004) concluded that the closure temperature for the U-Th-Pb system in allanite is likely >700 °C, well above the peak temperature reached in Lanzo. The slow diffusion of Pb in allanite has been indirectly confirmed by our recent investigation of allanite in a variety of metamorphic rocks (Gregory and Rubatto, unpublished data). It can thus be concluded that, in the Lanzo sample, both zircon and allanite record formation ages and not cooling ages.

Zircon and allanite occur in the rock in close textural relationships (Fig. 1). However, as demonstrated above, metamorphic zircon replaces magmatic relicts and thus association with a new metamorphic mineral like allanite is not necessarily significant. In addition, mutual inclusions are generally lacking: the zircon has inclusions of epidote, which contain an allanite component in only a few cases. Therefore, despite the textural relationships, it is not required that the metamorphic zircon and allanite formed at the same time, as indicated by their respective ages. Both metamorphic zircon and allanite include abundant Na-rich pyroxene with an overlapping variable composition (Fig. 7d). The inclusions of Na-rich pyroxene provide evidence that zircon and allanite formed during the high-pressure stage, above the albite = jadeite + quartz equilibrium, i.e., >1.5 GPa at temperatures of 500–600 °C. Because the sample shows very little greenschist-facies retrogression it is unlikely that the allanite is a retrograde phase.

The trace-element composition and pattern of both minerals is in line with a high-pressure, subsolidus origin. The Ti-in-zircon thermometry (Watson et al. 2006) cannot be applied with confidence because the system is neither buffered by rutile (Ti) nor quartz (Si). The allanite is rich in Sr, which is expected in metamorphic allanite forming in the absence of plagioclase, a known sink for Sr. Minerals grown in the absence of plagioclase are expected to lack a negative Eu anomaly. The weak negative Eu anomaly in zircon and allanite of the Lanzo sample is likely inherited from the bulk-rock composition, as shown by bulk-rock analyses of various plagiogranites in different ophiolitic bodies (Kaczmarek et al. 2008).

The above lines of evidence suggest that zircon and allanite preserve different snapshots in the high-*P* history of the sample. This reasoning implies that the Lanzo meta-plagiogranite remained at high *P* for an extended period of time, on the order of 8 m.y.

Geological implications

According to the evidence presented above, the Lanzo meta-plagiogranite recorded Alpine metamorphism at relatively high pressures (>1.5 GPa) between ~55 and 46.5 Ma. This period of time is within what is reported for high-*P* metamorphism in other nearby units. The Sesia-Lanzo zone, immediately north of the Lanzo massif, is host to the oldest Alpine eclogites in the western Alps, which have been dated at ~65 Ma (e.g., Liermann et al. 2002; Rubatto et al. 1999). To the west, the Lanzo massif is in tectonic contact with ophiolitic sequences that are remnants of the Piemontese Ocean. Most segments of this unit record subduction-related metamorphism at around ~45 Ma with a range of ages between 50 and 38 Ma encompassing Sm-Nd and Lu-Hf on garnet (Amato et al. 1999; Dûchene et al. 1997; Lapen et al. 2003), U-Pb on zircon (Rubatto et al. 1998; Rubatto and Hermann 2003), Ar-Ar on phengite (Gouzu et al. 2006), and Rb-Sr on phengite (Amato et al. 1999; Cliff et al. 1998). In the locality of Lago di Cignana, within the ultrahigh-*P* unit of the Zermatt-Saas ophiolites, the spread in ages is encompassed by garnet (48.8 ± 2.1 to 40.6 ± 2.6 Ma; Amato et al. 1999; Lapen et al. 2003) and was interpreted by Lapen (2003) as due to protracted garnet growth during prograde, high-pressure metamorphism. A similar case is presented by the Lanzo sample, where minerals that grew at different stages (zircon and allanite) during subduction constrain the duration of the process (~8 m.y.).

Acknowledgments

The Electron Microprobe Unit at ANU is thanked for access to the SEM, and Frank Brink for assistance with EBSD analysis. This work benefited from discussions with Jörg Hermann, Mary-Alix Kaczmarek, and Alfons Berger. A. Putnis and D.J. Dunkley provided helpful reviews. D.R. acknowledges the financial support of the Australian Research Council (DP0556700) and O.M. the support of the Swiss National Science Foundation (PP002-102809).

References cited

Amato, J.M., Johnson, C.M., Baumgartner, L.P., and Beard, B.L. (1999) Rapid exhumation of the Zermatt-Saas ophiolite deduced from high-precision Sm-Nd and Rb-Sr geochronology. Earth and Planetary Science Letters, 171, 425–438.

Ayers, J.C. and Watson, B.E. (1991) Solubility of apatite, monazite, zircon, and rutile in supercritical aqueous fluids with implications for subduction zone geochemistry. Philosophical Transactions of the Royal Society of London Series A: Mathematical Physical and Engineering Sciences, 335(1638), 365–375.

Barth, S., Oberli, F., and Meier, M. (1994) Th-Pb versus U-Pb isotope systematics in allanite from co-genetic rhyolite and granodiorite: Implications for geochronology. Earth and Planetary Science Letters, 124, 149–159.

Bingen, B., Austrheim, H., and Whitehouse, M. (2001) Ilmenite as a source of zirconium during high-grade metamorphism? Textural evidence from the Caledonides of Western Norway and implications for zircon geochronology. Journal of Petrology, 42, 355–375.

Black, L.P., Kamo, S.L., Allen, C.M., Aleinikoff, J.M., Davis, D.W., Korsch, R.J., and Foudoulis, C. (2003) TEMORA 1: a new zircon standard for Phanerozoic U-Pb geochronology. Chemical Geology, 200, 155–170.

Boudier, F. (1978) Structure and petrology of the Lanzo peridotite massif (Piedmont Alps). Geological Society of America Bulletin, 89, 1574–1591.

Boudier, F. and Nicolas, A. (1972) Fusion partielle gabbroïque dans la lherzolite de Lanzo (Alpes piémontaises). Schweizerische Mineralogische und Petrographische Mitteilungen, 52, 39–56.

Charoy, B. and Raimbault, L. (1994) Zr-, Th-, and REE-rich biotite differentiates in the A-type granite pluton of Suzhou (eastern China): The key role of fluorine. Journal of Petrology, 35, 919–962.

Cliff, R.A., Barnicoat, A.C., and Inger, S. (1998) Early Tertiary eclogite facies metamorphism in the Monviso Ophiolites. Journal of Metamorphic Geology, 16, 447–455.

Corfu, F., Hanchar, J.M., Hoskin, P.W.O., and Kinny, P.D. (2003) Atlas of zircon texture. In J.M. Hanchar and P.W.O. Hoskin, Eds., Zircon, 53, p. 469–500. Reviews in Mineralogy and Geochemistry, Mineralogical Society of America, Chantilly, Virginia.

Degeling, H., Eggins, S., and Ellis, D.J. (2001) Zr budget for metamorphic reactions, and the formation of zircon from garnet breakdown. Journal of Metamorphic Geology, 65, 749–758.
Dûchene, S., Blichert-Toft, J., Luais, B., Télouk, P., Lardeaux, J.-M., and Albarède, F. (1997) The Lu-Hf dating of garnets and the ages of the Alpine high-pressure metamorphism. Nature, 387, 586–589.
Eggins, S.M., Rudnick, R.L., and McDonough, W.F. (1998) The composition of peridotites and their minerals: A laser ablation ICP-MS study. Earth and Planetary Science Letters, 154, 53–71.
Ewing, R.C., Meldrum, A., Wang, L., and Wang, S. (2000) Radiation-induced amorphization. In S.A.T. Redfern and M.A. Carpenter, Eds., Transformation Processes in Minerals, 39, p. 319–354. Reviews in Mineralogy and Geochemistry, Mineralogical Society of America, Chantilly, Virginia.
Geisler, T., Pidgeon, R.T., Kurtz, R., van Bronswijk, W., and Schleicher, H. (2003a) Experimental hydrothermal alteration of partially metamict zircon. American Mineralogist, 88, 1496–1543.
Geisler, T., Zhang, M., and Salje, E.K.H. (2003b) Recrystallization of almost fully amorphous zircon under hydrothermal conditions: An infrared spectroscopic study. Journal of Nuclear Materials, 320, 280–291.
Geisler, T., Schaltegger, U., and Tomaschek, F. (2007) Re-equilibration of zircon in acqueous fluids and melts. Elements, 3, 43–50.
Gouzu, C., Itaya, T., Hyodo, H., and Matsuda, T. (2006) Excess ^{40}Ar-free phengite in ultrahigh-pressure metamorphic rocks from the Lago di Cignana area, Western Alps. Lithos, 92, 418–430.
Gregory, C., Rubatto, D., Allen, C., Williams, I.S., Hermann, J., and Ireland, T. (2007) Allanite micro-geochronology: A LA-ICP-MS and SHRIMP U-Th-Pb study. Chemical Geology, 245, 162–182.
Hanchar, J.M. and Miller, C.F. (1993) Zircon zonation patterns as revealed by cathodoluminescence and backscattered electron images: Implications for interpretation of complex crustal histories. Chemical Geology, 110, 1–13.
Harley, S.L., Kelly, N.M., and Möller, A. (2007) Zircon behavior and the thermal histories of mountain chains. Elements, 3, 25–30.
Harlov, D.E., Wirth, R., and Forster, H.J. (2005) An experimental study of dissolution-reprecipitation in fluorapatite: Fluid infiltration and the formation of monazite. Contributions to Mineralogy and Petrology, 150, 268–286.
Hazen, R.M. and Finger, L.W. (1979) Crystal-structure and compressibility of zircon at high-pressure. American Mineralogist, 64, 196–201.
Hoskin, P.W.O. and Black, L.P. (2000) Metamorphic zircon formation by solid-state recrystallization of protolith igneous zircon. Journal of Metamorphic Geology, 18, 423–439.
Kaczmarek, M.-A., Müntener, O., and Rubatto, D. (2008) Trace element chemistry and U-Pb dating of zircons from oceanic gabbros and their relationship with whole rock composition (Lanzo, Italian Alps). Contributions to Mineralogy and Petrology, 155, 295–312.
Kienast, J.R. and Pognante, U. (1988) Chloritoid-bearing assemblages in eclogitized metagabbros of the Lanzo peridotite body (Western Italian Alps). Lithos, 21, 1–11.
Lagabrielle, Y., Fudral, S., and Kienast, J.R. (1989) La couverture océanique des ultrabasites de Lanzo (Alpes occidentales): Arguments lithostratigraphiques et pétrologiques or [the oceanic cover of the Lanzo peridotite body (Western Italian Alps): Lithostratigraphic and petrological evidences]. Geodinamica Acta, 3, 43–55.
Lapen, T.J., Johnson, C.M., Baumgartner, L.P., Mahlen, N.J., Beard, B.L., and Amato, J.M. (2003) Burial rates during prograde metamorphism of an ultra-high-pressure terrane: An example from Lago di Cignana, western Alps, Italy. Earth and Planetary Science Letters, 215, 57–72.
Liermann, H.-P., Isachsen, C., Altenberger, U., and Oberhänsli, R. (2002) Behavior of zircon during high-pressure, low-temperature metamorphism: Case study from the Internal Unit of the Sesia Zone (western Italian Alps). European Journal of Mineralogy, 14, 61–71.
Ludwig, K.R. (2003) Isoplot/Ex version 3.0. A geochronological toolkit for Microsoft Excel, p. 70. Berkeley Geochronological Centre Special Publication, California.
Manning, C.E. (2004) The chemistry of subduction-zone fluids. Earth and Planetary Science Letters, 223, 1–16.
Müntener, O. and Piccardo, G.B. (2003) Melt migration in ophiolitic peridotites: The message from Alpine-Apennine peridotites and implications for embryonic ocean basins. In Y. Dilek, and P.T. Robinson, Eds., Ophiolites in Earth History, 218, p. 69–89. Geological Society of London Special Publication, U.K.
Oberli, F., Meier, M., Berger, A., Rosenberg, C.L., and Giere, R. (2004) U-Th-Pb and ^{230}Th/^{238}U disequilibrium isotope systematics: Precise accessory mineral chronology and melt evolution tracing in the Alpine Bergell intrusion. Geochimica et Cosmochimica Acta, 68, 2543–2560.
Pelletier, L. and Müntener, O. (2006) High-pressure metamorphism of the Lanzo peridotite and its oceanic cover, and some consequences for the Seisa-Lanzo zone (northern Italian Alps). Lithos, 90, 111–130.
Piccardo, G.B., Müntener, O., and Zanetti, A. (2004) Alpine-Apennine ophiolitic peridotites: New concepts on their composition and evolution. Ofioliti, 29, 63–74.
Pidgeon, R.T. (1992) Recrystallisation of oscillatory zoned zircon: some geochronological and petrological implications. Contributions to Mineralogy and Petrology, 110, 463–472.
Pidgeon, R.T., O'Neil, J.R., and Silver, R.T. (1966) Uranium and lead isotopic stability in metamict zircon under experimental hydrothermal conditions. Science, 154, 1538–1540.
Pidgeon, R.T., Nemchin, A.A., and Hitchen, G.J. (1998) Internal structures of zircons from Archean granites from the Darling Range batholith: implications for zircon stability and the interpretation of zircon U-Pb ages. Contributions to Mineralogy and Petrology, 132, 288–299.
Putnis, A. (2002) Mineral replacement reactions: From macroscopic observations to microscopic mechanisms. Mineralogical Magazine, 66, 689–708.
Putnis, A. and Putnis, C.V. (2007) The mechanism of reequilibration of solids in the presence of a fluid phase. Journal of Solid State Chemistry, 180, 1783–1786.
Putnis, A., Tsukamoto, K., and Nishimura, Y. (2005) Direct observations of pseudomorphism: Compositional and textural evolution at a fluid-solid interface. American Mineralogist, 90, 1909–1912.
Rasmussen, B. (2005) Zircon growth in very low grade metasedimentary rocks: Evidence for zirconium mobility at ~250 °C. Contributions to Mineralogy and Petrology, 150, 146–155.
Reddy, S.M., Timms, N.E., Trimby, P., Kinny, P.D., Buchan, C., and Blake, K. (2006) Crystal-plastic deformation of zircon: A defect in the assumption of chemical robustness. Gelogy, 34, 257–260.
Reddy, S.M., Timms, N.E., and Eglington, B.M. (2008) Electron backscatter diffraction analysis of zircon: A systematic assessment of match unit characteristics and pattern indexing optimization. American Mineralogist, 93, 187–197.
Rubatto, D. (2002) Zircon trace element geochemistry: distribution coefficients and the link between U-Pb ages and metamorphism. Chemical Geology, 184, 123–138.
Rubatto, D. and Gebauer, D. (2000) Use of cathodoluminescence for U-Pb zircon dating by ion microprobe: Some examples from the Western Alps. In M. Pagel, V. Barbin, P. Blanc, and D. Ohnenstetter, Eds., Cathodoluminescence in Geosciences, p. 373–400. Springer, Berlin.
Rubatto, D. and Hermann, J. (2003) Zircon formation during fluid circulation in eclogites (Monviso, Western Alps): Implications for Zr and Hf budget in subduction zones. Geochimica et Cosmochimica Acta, 67, 2173–2187.
——— (2007) Zircon behavior in deeply subducted rocks. Elements, 3, 31–35.
Rubatto, D., Gebauer, D., and Fanning, M. (1998) Jurassic formation and Eocene subduction of the Zermatt-Saas-Fee ophiolites: Implications for the geodynamic evolution of the Central and Western Alps. Contributions to Mineralogy and Petrology, 132, 269–287.
Rubatto, D., Gebauer, D., and Compagnoni, R. (1999) Dating of eclogite-facies zircons: The age of Alpine metamorphism in the Sesia-Lanzo Zone (Western Alps). Earth and Planetary Science Letters, 167, 141–158.
Spandler, C., Hermann, J., and Rubatto, D. (2004) Exsolution of thortveitite, yttrialite, and xenotime during low temperature recrystallization of zircon from New Caledonia, and their significance for trace element incorporation in zircon. American Mineralogist, 89, 1795–1806.
Stacey, J.S. and Kramers, J.D. (1975) Approximation of terrestrial lead evolution by a two-stage model. Earth and Planetary Science Letters, 26, 207–221.
Tomaschek, F., Kennedy, A.K., Villa, I.M., Lagos, M., and Ballhaus, C. (2003) Zircons from Syros, Cyclades, Greece—Recrystallization and mobilization of zircon during high-pressure metamorphism. Journal of Petrology, 44, 1977–2002.
Vavra, G., Gebauer, D., Schmidt, R., and Compston, W. (1996) Multiple zircon growth and recrystallization during polyphase Late Carboniferous to Triassic metamorphism in granulites of the Ivrea Zone (Southern Alps): an ion microprobe (SHRIMP) study. Contributions to Mineralogy and Petrology, 122, 337–358.
Watson, B.E. and Harrison, M.T. (1983) Zircon saturation revisited: temperature and composition effects in a variety of crustal magma types. Earth and Planetary Science Letters, 64, 295–304.
Watson, B.E., Wark, D.A., and Thomas, J.B. (2006) Crystallization thermometers for zircon and rutile. Contributions to Mineralogy and Petrology, 151, 413–433.
Williams, I. (1998) U-Th-Pb geochronology by ion microprobe. In M.A. McKibben, W.C. Shanks III, and W.I. Ridley, Eds., Application of Microanalytical Techniques to Understanding Mineralizing Processes, 7, p. 1–35. Reviews in Economic Geology, Society of Economic Geologists, Littleton, Colorado.

MANUSCRIPT RECEIVED NOVEMBER 28, 2007
MANUSCRIPT ACCEPTED APRIL 4, 2008
MANUSCRIPT HANDLED BY DANIEL HARLOV